Electrochimica Acta 281 (2018) 665–675

Contents lists available at ScienceDirect

Electrochimica Acta

journal homepage: www.elsevier.com/locate/electacta

Modeling 3D-microbatteries based on carbon foams

Priit Priimägi [a], Habtom D. Asfaw [b], Shruti Srivastav [b], Heiki Kasemägi [a], Alvo Aabloo [a], Daniel Brandell [b], Vahur Zadin [a, *]

[a] IMS Lab, Institute of Technology, University of Tartu, Nooruse 1, 504 11, Tartu, Estonia
[b] Department of Chemistry - Ångström Laboratory, Uppsala University, Lägerhyddsvägen 1, Box 538, SE-751 21, Uppsala, Sweden

ARTICLE INFO

Article history:
Received 26 March 2018
Received in revised form
25 May 2018
Accepted 27 May 2018
Available online 31 May 2018

Keywords:
3D-microbatteries
Electrochemistry modeling
Finite element methodology
Carbon foam

ABSTRACT

Porous electrodes are considered attractive for potential use as 3D current collectors in Li-ion microbatteries. Carbon foams, in particular, can be coated with a variety of active materials to prepare electrodes which can maximize energy and power density simultaneously. Modeling such electrodes will aid the selection of microstructural parameters (e.g. porosity) required to optimize their electrochemical performance. Here, experimentally-validated Finite Element Methodology (FEM) is used to simulate a 3D Li-ion microbattery featuring a carbon foam electrode coated by layers of $LiFePO_4$ nanoparticles. The electrodes are cycled against Li-metal at various current densities, and the electrochemical data obtained are used to benchmark and parametrize the simulations. By systematic variation of the $LiFePO_4$ coating thickness and homogeneity and the foam substrate, it is revealed that $LiFePO_4$ exhibits a uniform delithiation process and that the electrochemical reactions favor particles closer to the carbon structure, which is due to the poor electrical conductivity of $LiFePO_4$. Therefore, the cell capacity (mAh cm^{-2}) per footprint area can be increased by using lower charging currents, smaller carbon macropore sizes and thicker $LiFePO_4$ coatings. The porous carbon structure provides an excellent template for loadings of $LiFePO_4$ material, which in turn allows using thicker coatings with improved cell performance.

1. Introduction

An ever-increasing trend in miniaturization of devices for medical applications, sensing and telecommunications has recently intensified the development of suitable integrated power sources [1]. So far, Li-ion microbatteries (MB) represent one of the most promising energy-dense electrochemistry appropriate for these devices. To meet the demand for high energy and high power density (per footprint area of 1 mm^2), MB based on 3-dimensional (3D) electrode architectures have emerged [2,3]. The key attributes of these electrodes are related to shorter Li-ion diffusion path lengths, increased working electrode surface area, and prolonged cell life due to limited mechanical stresses from Li^+ insertion and removal [4]. To date, a variety of electrode architectures [5–8], novel electrode morphologies [9,10], active materials [11,12] and fabrication techniques [13–15] for 3D-MB-s have received considerable attention [16–19].

Among the fabrication techniques considered, photolithography of vertically-standing micropillars and the electrodeposition of arrays of nano-rods through porous membranes constitutes one of the first techniques to be explored [20]. Thin layers of active materials and electrolytes can be deposited onto the 3D structures when manufacturing electrodes for MB applications [3,21]. A more novel approach is to use foam-type electrodes, e.g. nickel foam as 3D electrode [22,23] or foam-type materials as 3D current collectors to be coated with various active materials [24]. For instance, Asfaw et al. [25] has reported the successful fabrication of a 3D composite cathode comprising $LiFePO_4$ nanoparticles deposited conformally onto emulsion-templated carbon foams by sol-gel method.

Carbonaceous materials have long been used as negative active materials for rechargeable Li-ion batteries [26,27]. In recent years, there has been an increasing trend in the use of monolithic porous carbons as 3D electrodes or current collectors in Li-ion MB [28–30]. By virtue of its bicontinuous structure, a 3D electrode based on porous carbons promotes effective utilization of the active materials (e.g. $LiFePO_4$ coating) as it provides both continuous electronic and ionic conduction pathways through the entire depth of the electrode. The mechanical stiffness associated with the electrodes helps reduce the risk of detachment of active materials during

* Corresponding author.
E-mail address: vahur.zadin@ut.ee (V. Zadin).

https://doi.org/10.1016/j.electacta.2018.05.179

battery operation, which thus improves the cycle life of the batteries [25,31]. Furthermore, as the porous electrodes provide high specific surface areas for coating with the active material and, possibly, with a solid electrolyte, they have low local current densities and thus are well-suited for high rate cycling of active materials with minimal resistive losses.

The phospho-olivine $LiFePO_4$ cathode material is widely used in commercial products. It consists of plentiful constituents, is environmentally benign, abundant, low-cost, non-toxic and has a competitive theoretical capacity of 170 mAh g^{-1} [32]. The main disadvantage associated with $LiFePO_4$ is its poor electronic conductivity (~$5\cdot10^{-7}$ S m^{-1}) compared to other positive electrode materials [33]. One strategy to overcome this obstacle is to downsize the active material and to deposit it directly onto a surface of a porous carbon network, which will serve as a support and 3D current collector [25].

Various types of computational simulation methods have been used to gain better understanding of the electrochemical behavior and performance of electroactive materials in a rapid and cost-effective manner [34,35]. Theoretical tools like Density Functional Theory (DFT) calculations [36,37] and Molecular Dynamics (MD) [38,39] simulations are frequently used to study material properties at the electronic and atomistic scale. However, Finite Element Method (FEM) is the most successful approach when it comes to solving equations that describe transport and kinetic processes and hence is employed to simulate electrochemical devices at a cell level [40–44]. So far, only a few groups have tried to represent the electrochemical behavior of 3D-structured electrodes using 3D models [45–50]. Although those works have provided helpful insights into the non-uniformity of the electrochemical reactions which occur due to the 3D-architectures and suggested different strategies to mitigate these effects, it should be mentioned that most of these studies use assumptions to approximate the 3D electrodes using 1D transport models and have not used experimental comparisons.

We focus on half-cells based on $LiFePO_4$-coated 3D carbon foam cathodes, employed using lithium foil counter and reference electrodes [25]. An experimentally validated and parametrized model is first constructed to benchmark the electrochemical performance of the 3D-electrodes. Thereafter, we describe the effects of changing the geometrical parameters of the electrodes (i.e., the carbon foam macropore size, the $LiFePO_4$ coating thickness and the coating homogeneity), followed by studies where the current density is varied. These parametric simulations helps to suggest which 3D carbon geometrical parameters should improve battery performance. The voltage-charge capacity profiles and cell capacity, current distribution, Li-ion concentration gradient in the electrolyte, and material utilization in the electrodes are analyzed.

2. Materials and methods

2.1. Geometrical model and material parameters

In this work, a cell MB where a thin film of nanosized $LiFePO_4$ particles are coated onto the walls of a carbon foam, working as a 3D composite nanoporous electrode (cathode) against a lithium metal foil electrode (anode), has been studied. The geometrical model used in these simulations is based on experimental work carried out by Asfaw et al. [25]. One cross-section image of the hierarchically structured composite electrode with an approximate thickness of 400 μm is shown in Fig. 1a. It was found that the mean diameter of the macro-pores in the carbon foam was around 20 μm (Fig. 1b), which is equivalent to 50 voids per a millimeter [25]. At higher magnification, the SEM images reveal details of the roughness of the walls of the $LiFePO_4$-coated carbon foam, also displaying the interconnectivities (Fig. 1d). The coating thickness was estimated to be roughly 175 nm [25]. For comparison, the 3D visualization of the $LiFePO_4$ coated carbon foam used in the computer model is shown in Fig. 1c.

The length of the complete simulation cell of the reference system was chosen to be 57.5 μm and is presented in Fig. 2. Grey domains represent the carbon structure with a length of 52 μm, which is roughly 1/8 of the electrode thicknesses used in the experiments (400 μm) to compromise computational cost and accuracy [25]. The surface of the carbon foam is coated with a thin (200 nm) layer of the $LiFePO_4$ nanoparticles (blue) while the Li-metal electrode (green) has a thickness of 0.5 μm. The remaining volume of the cell is filled with a liquid electrolyte (1 M $LiPF_6$ in ethylene carbonate (EC): diethyl carbonate (DEC) in a 1:1 wt ratio) as in the experiments. Since, separator usually have high and constant ionic transportation parameters then no separator was used in these half-cell simulations.

2.2. Mathematical model

The applied electrochemical battery model is based on the concentrated solution and porous electrode theories, established for Li-ion batteries and originally developed by Newman's group [51,52]. The mass transport in the electrolyte originates from Stefan-Maxwell multicomponent diffusion equation where Bruggeman's relation was used for effective ionic diffusion coefficient and ionic conductivity of the electrolyte in the electrode pores [53,54]. Also mass transport in the porous $LiFePO_4$ electrode, coating on the carbon foam, is corrected with Bruggeman's effective electronic conductivity while diffusion is based on Fick's diffusion law [54]. The electrochemical kinetics of the electrode reactions are defined by the Butler-Volmer equation [53,55]:

$$J = i_0\left[\exp\left(\frac{\alpha_a F\eta}{RT}\right) - \exp\left(-\frac{\alpha_c F\eta}{RT}\right)\right] \quad (1)$$

where J represents the total rate of ion exchange as current density (A m^{-2}), i_0 is exchange current density (A m^{-2}), F is Faraday's constant (C mol^{-1}), R is the universal gas constant (J K^{-1} mol^{-1}), T is temperature (K), $\alpha_a = \alpha_c = 0.5$ are anodic and cathodic transfer coefficients, respectively, and the surface overpotential η during discharge is described as:

$$\eta = \varphi_1 - \varphi_2 - U_{OC} \quad (2)$$

where φ_1 is the potential in the electrode, φ_2 is the potential in the electrolyte and the open circuit potential U_{oc} of the electrode is a fitted function obtained from literature [56,57]. The exchange current density in Eq. (1) can be calculated according to:

$$i_0 = F(k_a)^{\alpha_c}(k_c)^{\alpha_a}\left(c_{s,max} - c_s\right)^{\alpha_a}(c_s)^{\alpha_c}(c)^{\alpha_a} \quad (3)$$

Where k_a and k_c are anodic and cathodic rate constants (m s^{-1}), c_s and c are the Li-ion concentration in solid phase and in the electrolyte, respectively. More detailed description of mathematical model can be found in our previous studies of designing 3D-pillar MB-s and thermal analysis of MB-s [46,48].

2.3. Model construction and validation

In the current study, in order to increase the computational efficiency, the periodic nature in the spatial directions of the given carbon foam was used and 1/8 of the experimental electrode thickness was modeled. Since the foam electrode is highly porous (defined as macropores in these simulation cells) then it is assumed

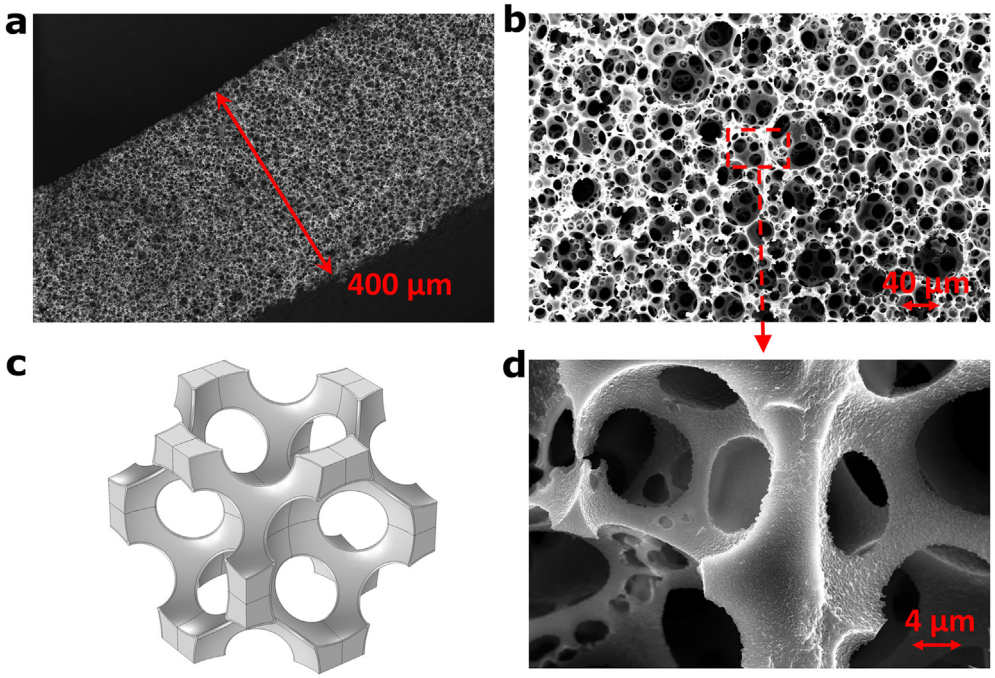

Fig. 1. (a) A slice of the foam type electrode, approximately 400 µm in thickness and coated with a thin layer of $LiFePO_4$ [25]. Micrographs (b) and (d) represent the coated carbon foam at higher magnification. (c) Computer model of the carbon foam structure with a 200 nm thick $LiFePO_4$ coating. Adapted from Ref. [25] with permission from The Royal Society of Chemistry.

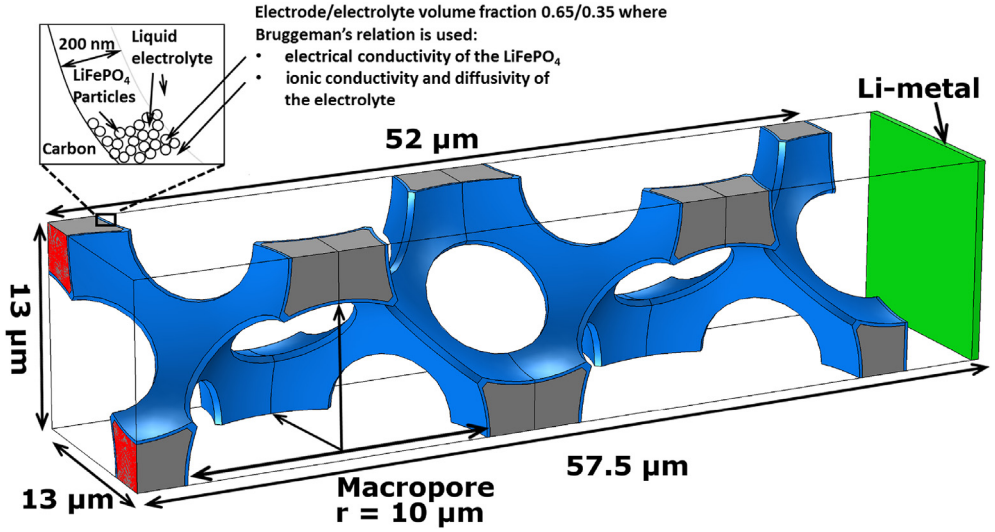

Fig. 2. The simulated cell, grey: the carbon structure with a radius of macropores r = 10 µm, blue: 200 nm thick nanoporous $LiFePO_4$ coating, green: Li-metal sheet. The rest of the volume is filled with liquid electrolyte (1 M $LiPF_6$ in 1:1 EC:DEC) and the area of applied current to the cell is marked red. (For interpretation of the references to color in this figure legend, the reader is referred to the Web version of this article.)

that electrolyte have good access in the foam and likewise a high electrochemical interaction interface due to the high surface area. Also, since the carbon electrical conductivity and diffusion coefficient of the $LiFePO_4$ are constant, the transportation limitations and resistance can be assumed to be a linear function in depth of the foam electrode. Accordingly, the applied current density ($0.37\ mA\ cm^{-2}$) in the simulations corresponds to 1/8 of the experimental values ($3\ mA\ cm^{-2}$). In each model, the current density $0.37\ mA\ cm^{-2} = 3.7\ A\ m^{-2}$ was applied to the surface area ($2.045 \cdot 10^{-11}\ m^2$ in the reference system) of the carbon structure which is actually in contact with the current collector, shown in red in Fig. 2. The opposing current collector at the lithium metal side was grounded. The average size for majority of the $LiFePO_4$ particles (above 80%) was measured to be below 70 nm, and therefore an average particle diameter of 20 nm was used in the simulations. The $LiFePO_4$ volume fraction, the electrolyte volume fraction and the double layer capacitance were measured or calculated from experimental data and are presented in Table 1. The electrolyte ionic conductivity ($S\ m^{-1}$) is represented by a concentration-dependent function based on the experimental data [58].

Fine-tuning of the mathematical model involves the setup of the charge voltage profile. This is achieved by determining the Li-metal

Table 1
Values of parameters used in the reference system.

	Name/description	Value	Unit	Ref.
T	Temperature	293.15	K	
c_0	Initial electrolyte salt concentration	1000	mol m^{-3}	
D_e	Electrolyte diffusion coefficient	$3 \cdot 10^{-10}$	m^2 s^{-1}	[56]
t_+	Electrolyte transport number	0.363	1	[56]
D_c	$LiFePO_4$ diffusion coefficient	$1 \cdot 10^{-12}$	m^2 s^{-1}	[61]
$c_{max,c}$	$LiFePO_4$ maximum species concentration	21190	mol m^{-3}	
r	Particle mean center-surface distance	10	nm	[25]
ε_e	Electrolyte volume fraction in the $LiFePO_4$ coating	0.35	1	[25]
ε_c	$LiFePO_4$ electrode volume fraction in the coating	0.65	1	[25]
ε_{foam}	Carbon foam volume fraction	~0.30	1	[25]
k_a, k_c	$LiFePO_4$ anodic and cathodic reaction rate constant	$7 \cdot 10^{-11}$	m s^{-1}	
c_c	$LiFePO_4$ electrical double layer capacitance	1	F m^{-2}	
α_a, α_c	$LiFePO_4$ and Li-metal anodic and cathodic transfer coefficients	0.5	1	[62]
σ_{Li}	Li-metal electrode electrical conductivity	$1 \cdot 10^{7}$	S m^{-1}	
k_{Li}	Li-metal anodic and cathodic reaction rate constant	$5 \cdot 10^{-7}$	m s^{-1}	
C_{Li}	Li-metal double layer capacitance	0.001	F m^{-2}	
σ_{carbon}	Carbon electrical conductivity	100	S m^{-1}	[63]

anodic and cathodic reaction rate constants by comparing experimental and simulation voltage profiles using least square fitting method [59].

$$\sqrt{\frac{1}{n}\sum_i [experiment(x_i) - simulation(x_i)]^2} < 5\% \quad (4)$$

A lower electronic conductivity of the $LiFePO_4$ for the delithiated phase ($FePO_4$) has also been reported in previous studies [60]. Therefore, the $LiFePO_4$ electrical conductivity was set to decrease linearly from the value of $1 \cdot 10^{-6}$ S m^{-1} in the lithiated $LiFePO_4$ phase down to the value of $1 \cdot 10^{-7}$ S m^{-1} in the delithiated $FePO_4$ phase while charging the cell. The coated carbon foam electrode soaked in liquid electrolyte has a volume fraction around ~0.30. The porous $LiFePO_4$ layer coated on the walls of carbon foam has a fixed 0.65/0.35 electrode/electrolyte fraction in all the simulations, and Bruggeman's approximation is used specifically for this layer. All other physical constants and parameters (electrolyte salt diffusion coefficient, electrolyte transport number, Li-ion diffusion coefficient in $LiFePO_4$, $LiFePO_4$ maximum species concentration, transfer coefficients, Li-metal electrical conductivity and carbon electrical conductivity) were found from literature and are presented in Table 1 with references.

The electrochemical behavior of this simulated material has been modeled using COMSOL Multiphysics 5.0. Applied model is based on the assumption that the salt in the electrolyte is completely dissociated. Initially, the electrolyte salt concentration was set to 1000 mol m^{-3} and the initial $LiFePO_4$ lithiation level was 99% in each simulation. In addition, the temperature was kept constant at 293.15 K and lithium insertion into carbon and other possible side reactions were neglected. In these time-dependent studies, a segregated non-linear calculation method and the linear MUMPS solver was used. Mesh consists of ~100 000–200 000 tetrahedral elements with additional elements between thin surfaces to catch the boundary effects.

2.4. Simulated systems

A total of 16 cell models were built. The first galvanostatic charge curves of these systems were simulated and studied in the potential range from 3 V to 4 V vs. Li^+/Li. In the first set, a parametric current density study was performed for 3 experimentally validated models, corresponding to the current densities 0.1, 1 and 3 mA cm^{-2}. A second set of simulations was carried out to investigate the effect of varying the $LiFePO_4$ coating thickness from 100 to 500 nm with increments of 100 nm. In addition, one simulated system with a non-uniform $LiFePO_4$ coating thickness varying from 200 nm to 600 nm was investigated to evaluate the insights of the homogeneity of the coating on the electrochemical performance of the electrode. Since the average size of the $LiFePO_4$ particles are less than 70 nm then particles with average diameter of 5, 10, 15, 20 and 40 nm were studied in the third part of the simulations to shed light on the role of particle size during cycling these 3D foam electrodes. Finally, two systems with different carbon voids (i.e., the macropore shown in Fig. 2), 5 and 10 μm radii-sized macropores, were simulated to collect the data about of the influence of the foam structure on the cell performance. Throughout the studies, only one parameter was changed in each system of the comparative set. Each parametric set also includes the reference system (with values presented in Table 1) for comparison.

3. Results and discussion

3.1. Charge characteristics of the simulated 3D half-cell and benchmarking towards experiments

The first single electrode system constructed and defined according to the experiment characteristics was named 'reference system', for which a current density of 3 mA cm^{-2} was used. The complete current density study includes 0.1, 1 and 3 mA cm^{-2}, which would roughly correspond to 0.06, 0.69 and 2.44 C-rates, respectively. The simulated voltage-capacity curves (Fig. 3) are in close agreement with the experimental data, which in turn indicates that the model can accurately simulate the mass and charge transport phenomena in these cells, and can hence be used to obtain reliable insights into the electrochemical behavior of the MB with the 3D foam type of electrode architecture.

The voltage-charge capacity curve recorded at the current density of 0.1 mA cm^{-2} exhibit a distinct plateau around 3.45 V, which is characteristic of cells containing $LiFePO_4$ active material [60,64,65]. Lower current densities surely provide lower local currents in the $LiFePO_4$-coated electrodes and thus a smoother and deeper delithiation, which accordingly increase the gravimetric capacity (mAh g^{-1}) per gram of $LiFePO_4$. For example, when decreasing the current density from 3 mA cm^{-2} down to 0.1 mA cm^{-2}, the cell capacity increases from 118 mAh g^{-1} to 160 mAh g^{-1}, i.e. 36% and forms 94% of the $LiFePO_4$ theoretical capacity (170 mAh g^{-1}). This effect is directly related to the fact that increased current densities cause higher voltage drops and kinetic overpotentials which limits the working voltage window, and thus

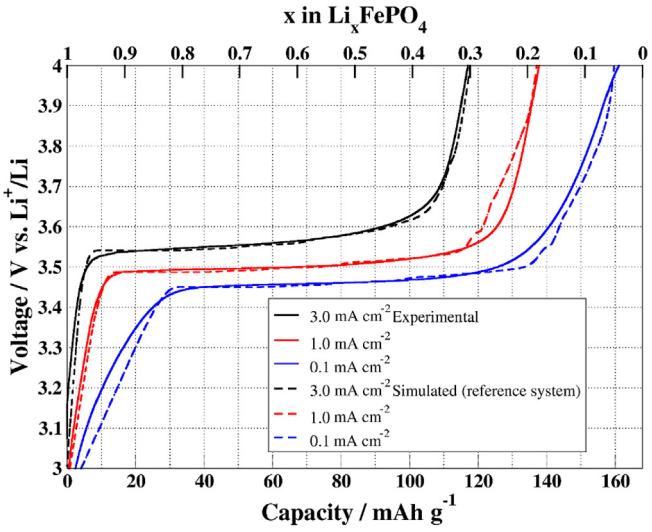

Fig. 3. The voltage-charge capacity profiles of $LiFePO_4$-coated carbon foam at different current densities in the charge cycle within a voltage range from 3 V to 4 V. The solid lines represent experimental data [25] and the dotted lines indicate the simulation results. The upper horizontal axis shows the degree of delithiation (x in Li_xFePO_4) in the $LiFePO_4$ electrode and the lower horizontal axis gives the cell capacity (mAh g^{-1}).

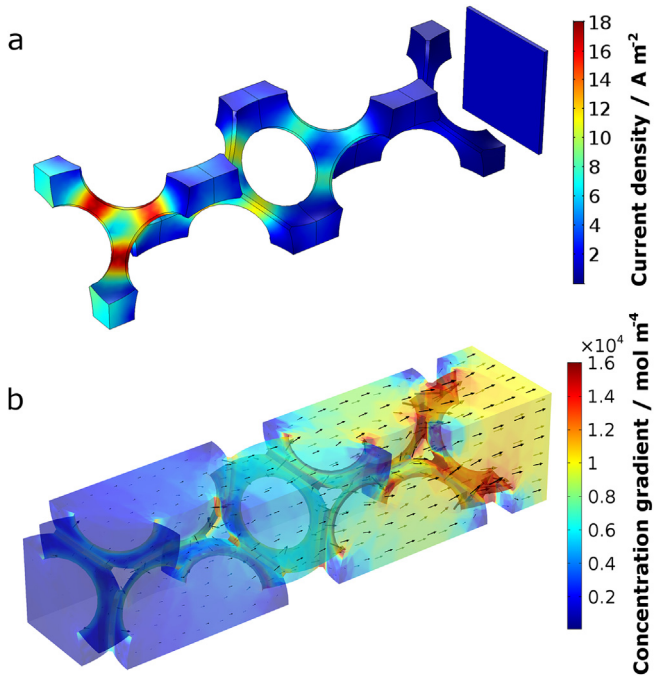

Fig. 4. Simulation snapshots taken at the end of the charge: (a) Current density (A m^{-2}) in the carbon foam structure; (b) Li-ion concentration gradient (mol m^{-4}) in the electrolyte with arrows proportionally showing the decreasing direction of the Li-ion concentration gradient.

limit the accessibility of the active materials during cycling (as also discussed below).

Another interesting observation is that the simulated potential profiles appears to have more linear features at the beginning and end of charging, as compared to experimental data (Fig. 3). This effect might be caused by the simplistic and perfectly homogeneous $LiFePO_4$-coating of the carbon foam structure (Fig. 1c) used in these simulations, as compared to the experimental materials (Fig. 1b and d). Since the simulations do not capture any roughness of the electrode surface, this indicate that imperfections might be present in the experimental system.

When comparing the depth of delithiation (Fig. 3) for different current densities, there is a tendency that a lower level of delithiation ($Li_{0.04}FePO_4$) is achieved for lower C-rates (0.06 C). The highest C-rate (2.44 C) provides only delithiation to $Li_{0.3}FePO_4$ at the end of the charge. Therefore, lower C-rates lead to a deeper delithiation, which in turn gives higher capacity. This is likely due to the sufficient diffusion in the electrolyte phase to maintain a uniform charging at all depths of the porous electrode only at low charge/discharge rates. If the charging rate is high, however, the electrolyte becomes polarized at the largest distance from the anode, which results in the impeded charging so that only the parts near the separator can participate fully in the charging process [66]. Moreover, the results obtained here are very similar to the SOC curves of $LiFePO_4$ [60,64], where a delithiation level $Li_{0.2}FePO_4$ was achieved using a C/10 rate.

3.2. Current density distribution and concentration gradients in the cell

In Fig. 4a, the current density (A m^{-2}) distribution in the carbon foam part of the simulated structure is presented, together with the Li-metal electrode. This particular snapshot is taken at the end of the charging, but is representative for the entire charging process since the applied current density is constant. The oxidation reaction in $LiFePO_4$ during charging progress as the material is delithiated (i.e., Li_xFePO_4 and $x = 1 \rightarrow 0$) and can be expressed as:

$$LiFePO_4 \rightarrow FePO_4 + Li^+ + e^- \quad (5)$$

Here a two-phase model ($LiFePO_4$ as lithiated and $FePO_4$ as delithiated phase) with non-stoichiometric compositions is used, which represents the average phase for certain region or the entire electrode. In the course of the above reaction, all electrons are transferred to the electronically well-conductive (100 S m^{-1}, which is several orders of magnitude higher than the electronic conductivity of $LiFePO_4$) carbon structure where they continue moving towards the current collector.

Fig. 4a shows the situation where the highest C-rate (2.44), which corresponds to the current density of 3.7 A m^{-2} used in the reference cell. However, the highest current density (~19 A m^{-2}) that the carbon foam structure has to support is located in the narrow regions near the current collector. The electrons released into the carbon from $LiFePO_4$ migrate towards the current collector, and the narrow carbon structure regions in its vicinity are therefore exposed to high currents and thus high current densities. This can give rise to the local overheating of these regions of the battery, and is an inherent effect of the highly porous structure of the carbon foam composite electrode [4].

In Fig. 4b, the Li-ion concentration gradient (mol m^{-4}) in the electrolyte at the end of the charging process is presented. It can be noticed that the concentration gradient in the liquid electrolyte is higher in regions closer to the counter electrode (Li-metal). This effect is equivalent to a higher rate of changing Li-ion concentration in these regions. In addition, the black arrows in Fig. 4b represents the direction of the diffusive flux of Li-ions, thereby showing the direction of decreasing concentration. The length of the arrows proportionally displays the changes in the concentration gradient. At constant charging current, there is a constant flux of Li-ions from the $LiFePO_4$ into the electrolyte. When the Li-ions are inserted into the Li-metal electrode, this causes a small deficit of Li-ions and a somewhat lower concentration near this surface, and the Li-ions are migrating towards these lower concentration regions. This effect of a higher gradient closer to the Li-metal remains almost unchanged during the entire charging process, as the current

density (3.7 A cm^{-2}) is constant and the delithiation of the $LiFePO_4$ layer is highly uniform (also discussed in section 3.3).

3.3. *$LiFePO_4$ delithiation and coating homogeneity*

In this part of the study, the phase evolution of a non-uniform $LiFePO_4$-coated carbon foam electrode is analyzed, for coating thicknesses varying from 600 to 200 nm. In Fig. 5, the depth of delithiation in the $LiFePO_4$ electrode (x in Li_xFePO_4) after 1500 s of charging at 2.44 C-rate is shown. It can be noticed that the electrochemical delithiation reaction ($LiFePO_4 \rightarrow FePO_4 + Li^+ + e^-$) occurs preferentially in the particles that are closer to the carbon structure than in particles closer to the electrolyte. After 1500 s of charging, these regions are almost entirely delithiated and are seen as blue in Fig. 5.

The development of the delithiated phase is seen in better detail in Fig. 6. These cross-section snapshots of the electrode illustrate the progress of the delithiation as a function of time intervals during cell charging from 3 V to 4 V. The non-uniform $LiFePO_4$ coating on the carbon foam structure presents different coating consistencies and thicknesses: (a) a thin (200 nm) homogeneous coating, (b) a coating where edges and tips of the $LiFePO_4$ layer are somewhat thicker, (c) a coating where one side of the carbon has thicker coating than the other, and (d) a thick (600 nm) homogeneous coating. It is clearly seen that the $LiFePO_4$ particles near the carbon foam, in the bottom of the coating layer, are delithiated first while the chemical reaction progresses in the $LiFePO_4$ bulk layer within the time interval between 2000 and 4000 s for all investigated systems. At later charging stages (i.e., at 6000 s), it can be seen that regions with thinner $LiFePO_4$ coatings are fully delithiated but that the thicker regions (the edges on row *b* and the surfaces on *c* and *d*) remain lithiated. The major limiting factor for the electrochemical process in this system is the significantly lower electrical conductivity of the $LiFePO_4$ phase (~$5 \cdot 10^{-7}$ S m^{-1}) compared to carbon foam. When Li-ions and electrons are extracted from the $LiFePO_4$ particles during delithiation, the carbon foam structure acts as a supportive highway for the released electrons to move towards the current collector, thereby favoring reactions in the $LiFePO_4$ particles in the coating near the carbon structure. This effect also has been reported by Strobridge et al. [67] who observed a preference for reactivity in $LiFePO_4$ particles closer to the current collector, which was explained by better wiring in this electrode region. Additionally, a lower and constant charging rate in the vicinity of a current collector generate a constant chemical reaction rate in the $LiFePO_4$, rendering a mostly homogeneous delithiated phase.

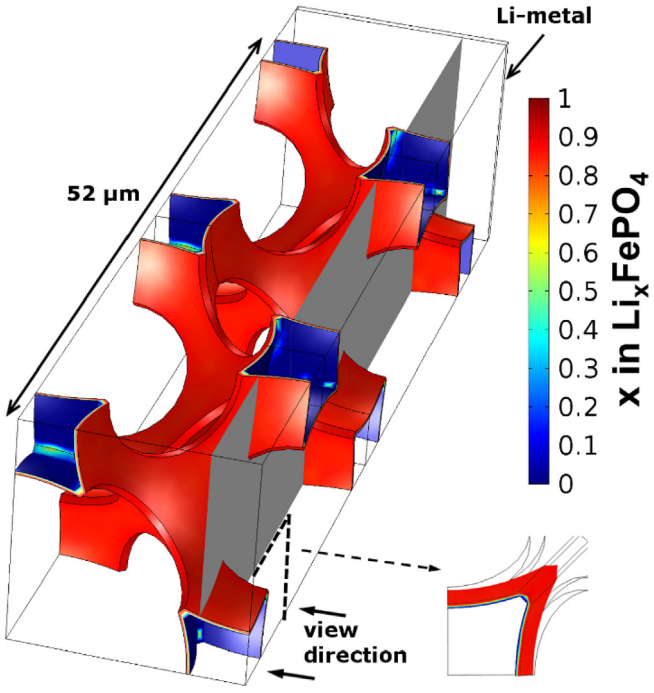

Fig. 5. Depth of delithiation in the $LiFePO_4$ electrode (as x in Li_xFePO_4) after 1500 s of charging for the reference system. The grey plane shows a cross-section of the $LiFePO_4$ electrode with point-of-view directions for the representation in Fig. 6.

It can also be seen in Fig. 5 that depth of delithiation in the $LiFePO_4$ is very similar in the regions near the Li-metal and near the regions where current is applied, indicating that the delithiation is rather homogeneous throughout the porous electrode. This is in contrast to Liu et al. [66] and Strobridge et al. [67] who studied the delithiation processes of $LiFePO_4$ composite electrodes using energy-dispersive X-ray diffraction (EDXRD) methodology, and found that the delithiation of $LiFePO_4$ starts in particles which are closer to the separator (Li-metal side) than in parts which are closer to the current collector. This inhomogeneity of the electrochemical reaction in the electrode suggests Li-diffusion limited kinetics in the electrolyte across the cathode [67,68]. On the other hand, the present study comprises a highly electronically conductive carbon foam as a 3D support and a liquid electrolyte with high ionic conductivity. Moreover, the simulated electrode has a thickness of only 52 µm, as compared to the approximately 285 µm thick electrode studied by Strobridge et al. Therefore, any effect of inhomogeneous delithiation of the electrode is less likely to occur in these present studies. In conclusion, the surprisingly highly homogeneous delithiation observed in the simulations is most likely caused by the high electrical conduction (100 S m^{-1}) of the carbon foam, the large macropores filled with electrolyte, the high enough ionic diffusivity ($3 \cdot 10^{-10}$ m^2 s^{-1}) of the electrolyte, and the low charging rates (C-rate 2.44).

3.4. *Variation of the $LiFePO_4$ coating thickness*

To investigate how the cell capacity and electrochemical performance in these 3D-foam electrodes depend on the thickness of the $LiFePO_4$ coating, five different homogeneously $LiFePO_4$-coated electrodes with thicknesses of 100–500 nm were simulated. The voltage-capacity profiles of the charging process in these systems are shown in Fig. 7a and b for the areal capacity and gravimetric capacity, respectively. As expected from the different mass loadings, the gravimetric capacity (mAh g^{-1}) per gram of $LiFePO_4$ varies less than capacity per footprint area for the different coating thicknesses (Fig. 7b). Fig. 7a shows clearly that thicker coatings will increase the cell performance, simply because more active electrode material is available. Therefore, a footprint area capacity of 3.09 mAh cm^{-2} is achieved for the thicker coating (500 nm) as compared to 0.59 mAh cm^{-2} for the 100 nm $LiFePO_4$ coating (Fig. 7a and Table 2). On the other hand, when the volume of the $LiFePO_4$ was increased by 479% when using thicker coating, the footprint area capacity increased by 424%. Thus, the cell capacity per footprint area is significantly improved throughout the investigated range, although slightly less is gained when increasing the thickness from 400 nm to 500 nm coating as compared to increasing thinner layers. In conclusion, thicker coatings are preferable in this system, provided that these are possible to achieve using the current carbon foam macropore sizes and by the current synthesis techniques. It can be possible that very thick coating at some point decreases the cell capacity due to the increased diffusion pathways and clogged pores. The coating thickness of 500 nm is still not limiting the performance of the cell.

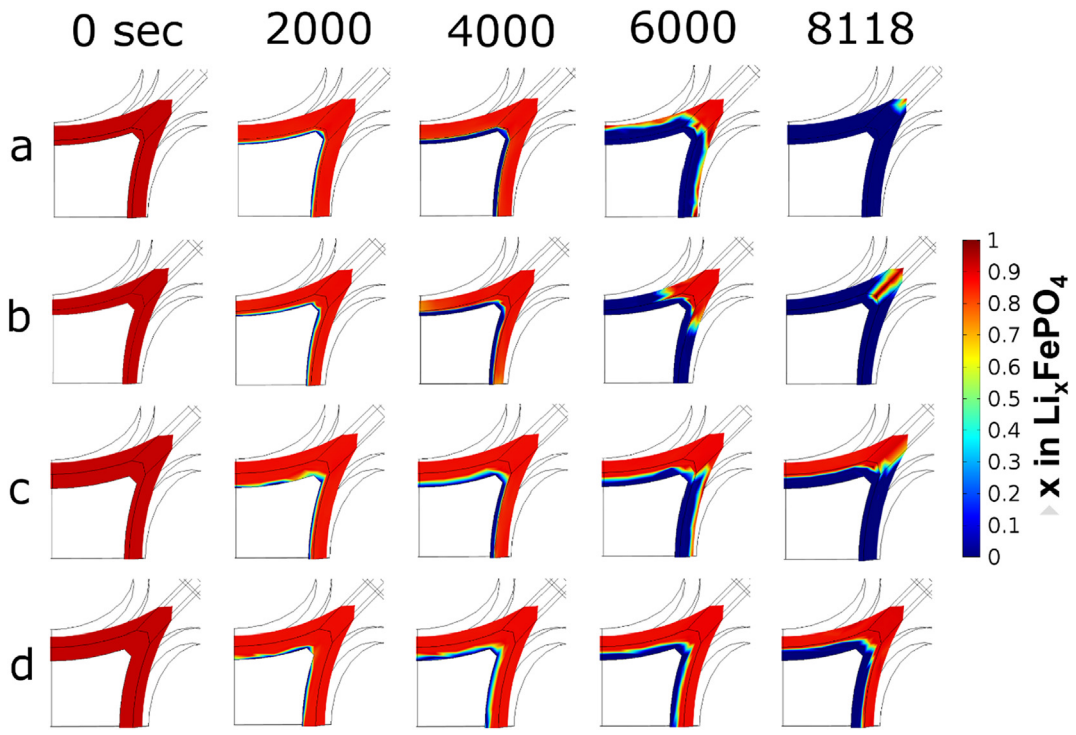

Fig. 6. 3D snapshots illustrating the degree of delithiation (x in Li_xFePO_4) in the electrode with different coating homogeneities during a charge cycle from 3 V (0 s) to 4 V (8118 s): (a) a thin (200 nm) homogeneous coating; (b) edges and tips of the $LiFePO_4$ are thicker; (c) one side of the carbon has thicker coating than the other; (d) a thick (600 nm) homogeneous coating. The grey lines represent the 3D carbon structure.

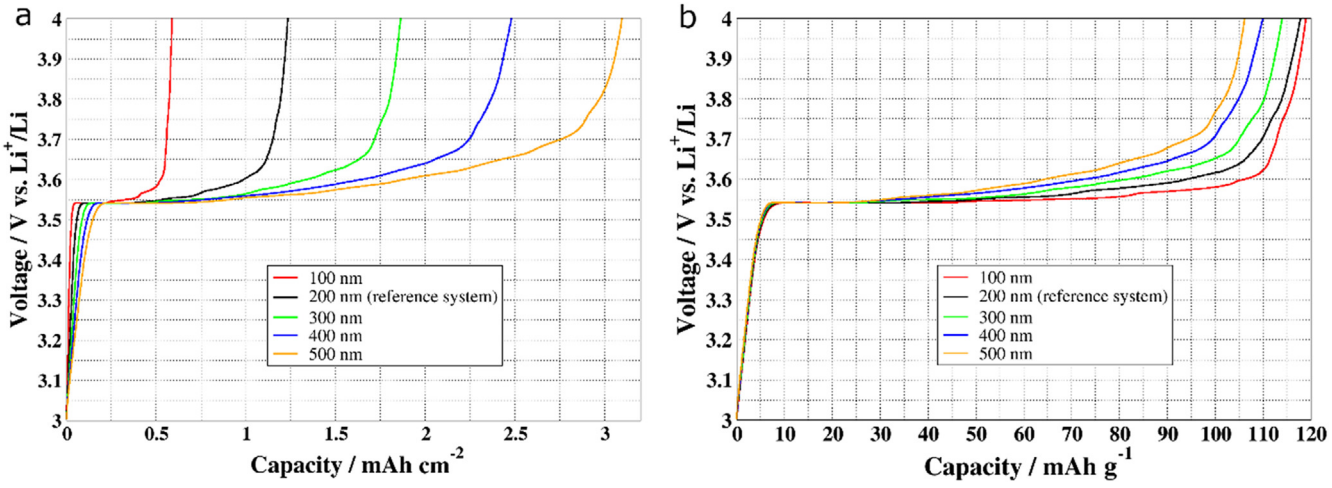

Fig. 7. The voltage-charge capacity profiles of $LiFePO_4$-coated carbon foam for different $LiFePO_4$ coating thicknesses in the range from 100 nm to 500 nm: (a) capacity per footprint area (mAh cm^{-2}), (b) gravimetric capacity (mAh g^{-1}) per gram of $LiFePO_4$.

Table 2
Geometrical characteristics and calculated capacities for different $LiFePO_4$ coating thickness.

Coating thickness/nm	$LiFePO_4$ volume/$\cdot 10^{-16}$ m^3	$LiFePO_4$ surface area/$\cdot 10^{-9}$ m^2	Capacity/mAh g^{-1}	Capacity/mAh cm^{-2}
100	1.38	2.46	119	0.59
200 (ref. system)	2.87	2.59	118	1.23
300	4.48	2.73	114	1.86
400	6.18	2.87	110	2.47
500	7.99	3.00	106	3.09

Upon closer examination of Fig. 7a, it can be seen that thinner coatings (100 nm and 200 nm) provides higher gravimetric capacity (119 and 118 mAh g^{-1}, respectively) than thicker (500 nm) coatings, which give 106 mAh g^{-1}. This tendency to a minor

decrease in gravimetric capacity per gram of $LiFePO_4$ is likely caused by the low electronic conductivity of $LiFePO_4$. Furthermore, this low conductivity possibly causes a faster potential rise in systems where a thicker coating was used. This rise of the ohmic polarization primarily originates from the resistance of the electrode material and the linear Ohm's law relationship between current and cell potential [69]. Hence, the thicker the coating of the $LiFePO_4$, the longer is the diffusion pathway from the lithium-rich particles to the electrolyte, and the active material delithiation thereby becomes limiting and the capacity decreases. These phenomena were also discussed previously in section 3.3. Therefore, increasing the electrical conductivity of the electrode material (e.g. coating the $LiFePO_4$ particles with highly conductive material), should hypothetically allow usage of thicker $LiFePO_4$ electrode films which would increase the cell capacity and allow applying higher charge/discharge rates.

3.5. Variation of the $LiFePO_4$ particle size

Furthermore, the influence of $LiFePO_4$ particle size (diameter of 5, 10, 15, 20 and 40 nm) on the cell electrochemical behavior was studied. In the porous electrode theory developed by Newman and Tiedemann [52,58], the electrode is treated as a one-dimensional continuous superposition of solid active material and liquid electrolyte phases, where the transport properties are corrected by the Bruggeman expressions [70]. In the following simulations the coating thickness (200 nm) and charging current density (3 mA cm^{-2}) were kept unchanged in all systems. Calculated gravimetric capacities for different electrode material particle sizes are presented in Fig. 8a. Since a relatively thin material coating (200 nm) was modeled, the particle size variation only resulted in minor capacity differences. However, it can be seen that smaller $LiFePO_4$ particles provided somewhat higher cell capacities. After the implementation of the porosity in the model, the decreased particle size effectively increases the electrode material volume ratio, and thereby the capacity increases. Moreover, Orvananos et al. [71] found that smaller particles provide a better rate performance compared to the larger particles due to their larger surface-to-volume ratio and smaller diffusion lengths for both ionic transport and electrical conduction [65]. In the delithiation process, Li-ions are more easily extracted from smaller particles rather than the larger particles, due to the length of the diffusion pathways and hence a lower overpotential is required. In addition, Li et al. [72] observed that since the Li-ion conduction channels within $LiFePO_4$ particles are one-dimensional, the diffusivity is mainly governed by the concentration of anti-site defects in these channels [73]. Therefore, larger particles reduce ion diffusivity and electronic conductivity of the material. The simulations here display similar effects being in a good agreement with several previous studies on the cell capacity dependency on the $LiFePO_4$ particle size [60,74,75].

3.6. Variation of the carbon foam macropore size

Clearly, the size of the macropores in the $LiFePO_4$-coated carbon foam (Fig. 1a and b) plays an important role in the performance of the electrochemical cell in which the 3D electrodes are used. In this section, a cathode with a macropores radius of 5 μm (Fig. 8b) is simulated and the results are compared with the reference system with macropore radius of 10 μm (Fig. 8c). A smaller macropore size will lead to an increased amount of carbon per identical volume of the simulation cell. This means that a larger coating area is available, and thereby $LiFePO_4$ electrode loading is higher. Direct comparisons of the electrochemical performances are thus difficult to make, although the contact areas between the current collector and the foam structure are equivalent in both systems.

The simulations showed that the increased (116%) $LiFePO_4$ loading volume resulted in an increase in capacity per footprint area (111%; from 1.23 up to 2.59 mAh cm^{-2}) when the radius of the

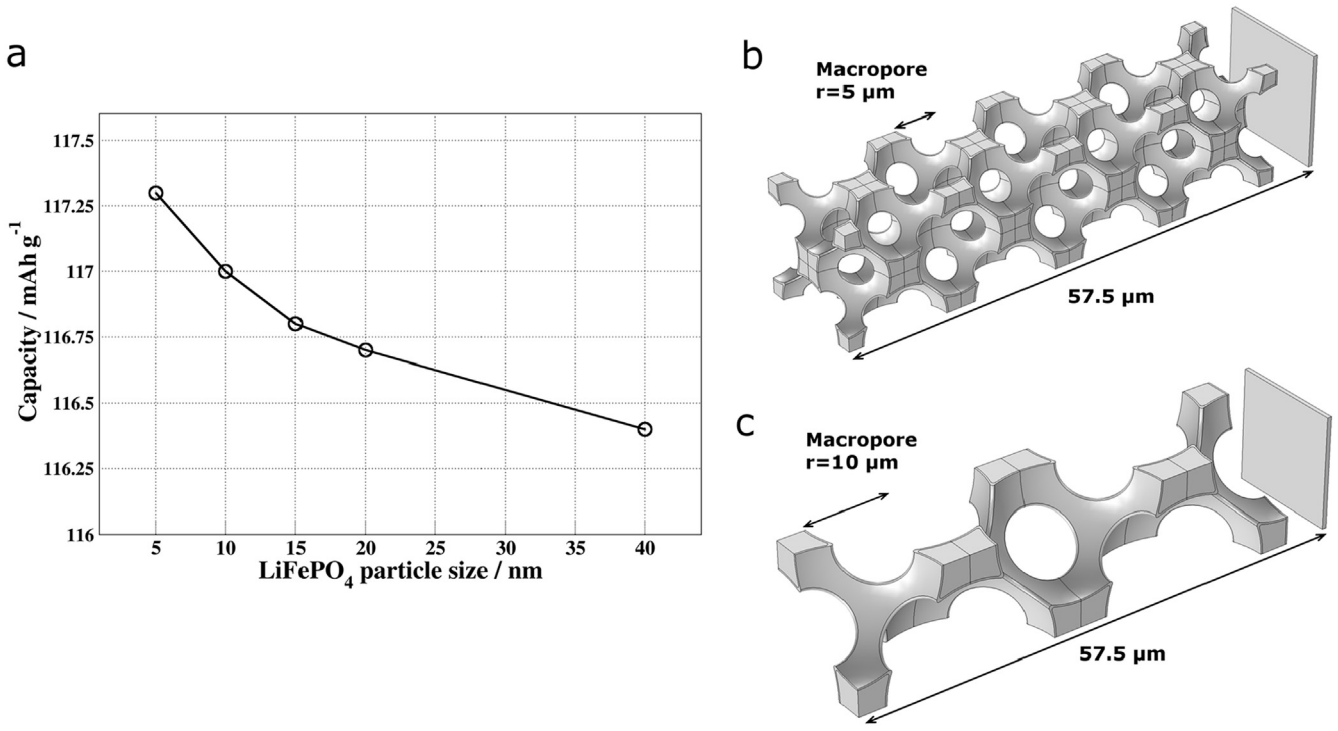

Fig. 8. (a) Simulated gravimetric capacity (mAh g^{-1}) per gram of $LiFePO_4$ for different $LiFePO_4$ particle sizes (marked as circles). (b) Simulation cell (length = 57.5 μm) with carbon foam macropore radii of 5 μm and (c) a reference system with macropore radii of 10 μm.

Table 3
Geometrical characteristics and calculated capacities for the reference system with macropore radii of 10 μm and for the system with macropore radii of 5 μm.

Macropore radius/μm	$LiFePO_4$ volume/$\cdot 10^{-16}$ m^3	$LiFePO_4$ surface area/$\cdot 10^{-9}$ m^2	Capacity/mAh g^{-1}	Capacity/mAh cm^{-2}	Max. current density in carbon/A m^{-2}
10 (ref. system)	2.87	2.59	118	1.23	18.9
5	6.19	5.55	115	2.59	19.1

macropores was reduced (Table 3). This capacity gain per footprint area stemming from the increased volume of the $LiFePO_4$ seems reasonable in the context of the results in section 3.4, and it can be concluded that using carbon foam with smaller macropores is the key for improving the battery performance when other parameters of the materials and the cell geometry remain unchanged. Also the gravimetric capacity of these cells remains largely unchanged. The carbon framework in the foam with smaller macropore size (Fig. 8b) has thinner and tight carbon regions than carbon foam structure with larger pores (Fig. 8c) to support locally high currents. Nevertheless, the simulations showed comparable current densities for carbon foam system with smaller macropore size (~19.1 A m^{-2}) and the reference system (18.9 A m^{-2}, corresponding to the red colored regions in Fig. 4a), because the cross-section area of the carbon is similar in both systems.

The Li-ion concentration gradient occurrence in the electrolyte and the delithiation distribution in the $LiFePO_4$ layer was similar in both smaller and larger macropore size systems. Accordingly, like in the reference system, the Li-ion concentration gradient in the electrolyte was observed to be higher in the regions near the Li-metal side. In addition, the delithiation of the $LiFePO_4$ was homogeneous in these systems and favorable in particles situated closer to the carbon structure, as discussed in section 3.3.

Only a small fraction of the material can be simulated by direct modeling of the 3D architecture simulation cell due to computational limitations. Since the two systems studied only showed minor limiting effects, however, also 10 times smaller macropores are likely to show similar results.

4. Conclusions

An experimentally-validated half-cell electrochemical system comprising a nano-sized $LiFePO_4$-coated carbon foam electrode was simulated first time, and parametric studies were successfully carried out. These calibrated models reveal insights into mass and ionic transport phenomena and suggest optimal electrode geometrical parameters to increase 3D MB capacity. Applying lower current density of 0.1 mA cm^{-2} provided smoother and deeper delithiation with about 36% increased cell gravimetric capacity (mAh g^{-1}) per gram of $LiFePO_4$ as compared to the higher current density 3 mA cm^{-2}. The simulations showed that the Li-ion concentration gradient is higher in the regions near the separator, but that the current density in the carbon foam is higher in the regions closer to the current collector. Both effects are associated with the higher ionic and electronic transports, respectively, observed in these regions. It is interesting to note that $LiFePO_4$ delithiation occurs homogeneously throughout the porous structure with the electrochemical reactions taking place preferably in the particles near the carbon foam due to the very low electrical conductivity (~$1 \cdot 10^{-7}$ S m^{-1}) of the $LiFePO_4$ coating. A certain suggestion for experimentalist is that carbon foam where exist smaller macropores, with increased available coating area and thicker coatings of the $LiFePO_4$, lead to an increased mass of available active material and thus enhanced cell capacity per footprint area. This shows that the porous carbon structure provides an excellent template for loadings of $LiFePO_4$ material in terms of current and electrolyte distribution, and any system limitations are hardly observed even for rather thick loadings. Therefore, this novel foam type electrodes can be a good candidate for improving the performance of 3D MB used in microelectromechanical systems.

Generally, the rate performance of a practical battery, and the reaction mechanism, are not merely a function of the size and morphology of the active materials, but as these studies demonstrate also depend strongly on the structure of the composite electrode and the resulting global electronic and ionic conductivities. Although the present study clearly shows that improvements in the cell performance can be achieved when lower current densities are used, carbon foam have smaller macropores and thicker coatings are applied, it is probably important to note that experimental capability to fabricate these composite electrodes with thick, homogeneous coatings may be a limiting factor.

Acknowledgements

This research was supported by the Estonian Research Council Grant PUT 1372, Estonian Science Foundation Grant ETF9216 and was conducted with support from the European Regional Development Fund. DB wishes to acknowledge the Carl Trygger foundation.

References

[1] F. Albano, M.D. Chung, D. Blaauw, D.M. Sylvester, K.D. Wise, A.M. Sastry, Design of an implantable power supply for an intraocular sensor, using POWER (power optimization for wireless energy requirements), J. Power Sources 170 (2007) 216–224, https://doi.org/10.1016/j.jpowsour.2007.04.007.
[2] T.S. Arthur, D.J. Bates, N. Cirigliano, D.C. Johnson, P. Malati, J.M. Mosby, et al., Three-dimensional electrodes and battery architectures, MRS Bull. 36 (2011) 523–531, https://doi.org/10.1557/mrs.2011.156.
[3] J.F.M. Oudenhoven, L. Baggetto, P.H.L. Notten, All-solid-State lithium-ion microbatteries: a review of various three-dimensional concepts, Adv. Energy Mater. 1 (2011) 10–33, https://doi.org/10.1002/aenm.201000002.
[4] V. Zadin, D. Brandell, H. Kasemägi, J. Lellep, A. Aabloo, Designing the 3D-microbattery geometry using the level-set method, J. Power Sources 244 (2013) 417–428, https://doi.org/10.1016/j.jpowsour.2012.12.004.
[5] B. Sun, D. Rehnlund, M.J. Lacey, D. Brandell, Electrodeposition of thin poly(-propylene glycol) acrylate electrolytes on 3D-nanopillar electrodes, Electrochim. Acta 137 (2014) 320–327, https://doi.org/10.1016/j.electacta.2014.06.008.
[6] G. Oltean, H. Desta Asfaw, L. Nyholm, K. Edstrom, A Li-Ion microbattery with 3D electrodes of different geometries, ECS Electrochem. Lett. 3 (2014) A54–A57, https://doi.org/10.1149/2.003406eel.
[7] N.S. Ergang, M. a. Fierke, Z. Wang, W.H. Smyrl, A. Stein, Fabrication of a fully infiltrated three-dimensional solid-state interpenetrating electrochemical cell, J. Electrochem. Soc. 154 (2007) A1135–A1139, https://doi.org/10.1149/1.2794288.
[8] M. Roberts, P. Johns, J. Owen, D. Brandell, K. Edstrom, G. El Enany, et al., 3D lithium ion batteries—from fundamentals to fabrication, J. Mater. Chem. 21 (2011) 9876–9890, https://doi.org/10.1039/c0jm04396f.
[9] G. Oltean, L. Nyholm, K. Edström, Galvanostatic electrodeposition of aluminium nano-rods for Li-ion three-dimensional micro-battery current collectors, Electrochim. Acta 56 (2011) 3203–3208, https://doi.org/10.1016/j.electacta.2011.01.053.
[10] D. Rehnlund, M. Valvo, C.-W. Tai, J. Ångström, M. Sahlberg, K. Edström, et al., Electrochemical fabrication and characterization of Cu/Cu2O multi-layered micro and nanorods in Li-ion batteries, Nanoscale 7 (2015) 13591–13604, https://doi.org/10.1039/C5NR03472H.
[11] S. Tan, S. Walus, T. Gustafsson, D. Brandell, 3-D microbattery electrolyte by self-assembly of oligomers, Solid State Ionics 198 (2011) 26–31, https://doi.org/10.1016/j.ssi.2011.07.005.
[12] J. Mindemark, B. Sun, D. Brandell, Hydroxyl-functionalized poly(trimethylene carbonate) electrolytes for 3D-electrode configurations, Polym. Chem. 6 (2015) 4766–4774, https://doi.org/10.1039/C5PY00446B.
[13] Y. Wang, W.D. Richards, S.P. Ong, L.J. Miara, J.C. Kim, Design principles for

solid-state lithium superionic conductors, Nat. Mater. 14 (2015) 1026–1032, https://doi.org/10.1038/NMAT4369.
[14] F. Chamran, Y. Yeh, H.-S. Min, B. Dunn, C.-J. Kim, Fabrication of high-aspect-ratio electrode arrays for three-dimensional microbatteries, J. Microelectromech. Syst. 16 (2007) 844–852, https://doi.org/10.1109/JMEMS.2007.901638.
[15] A. Vu, Y. Qian, A. Stein, Porous electrode materials for lithium-ion batteries - how to prepare them and what makes them special, Adv. Energy Mater. 2 (2012) 1056–1085, https://doi.org/10.1002/aenm.201200320.
[16] H. Zhang, X. Yu, P.V. Braun, Three-dimensional bicontinuous ultrafast-charge and -discharge bulk battery electrodes, Nat. Nanotechnol. 6 (2011) 277–281, https://doi.org/10.1038/nnano.2011.38.
[17] J.H. Pikul, H. Gang Zhang, J. Cho, P.V. Braun, W.P. King, High-power lithium ion microbatteries from interdigitated three-dimensional bicontinuous nanoporous electrodes, Nat. Commun. 4 (2013) 1732–1736, https://doi.org/10.1038/ncomms2747.
[18] M. Valvo, M. Roberts, G. Oltean, B. Sun, D. Rehnlund, D. Brandell, et al., Electrochemical elaboration of electrodes and electrolytes for 3D structured batteries, J. Mater. Chem. A. 1 (2013) 9281–9293, https://doi.org/10.1039/c3ta11921a.
[19] P. Johns, M. Roberts, J. Owen, Conformal electrodeposition of manganese dioxide onto reticulated vitreous carbon for 3D microbattery applications, J. Mater. Chem. 21 (2011) 10153, https://doi.org/10.1039/c0jm04357e.
[20] J.W. Long, B. Dunn, D.R. Rolison, H.S. White, Three-dimensional battery architectures, Chem. Rev. 104 (2004) 4463–4492, https://doi.org/10.1021/cr020740l.
[21] G.T. Teixidor, R.B. Zaouk, B.Y. Park, M.J. Madou, Fabrication and characterization of three-dimensional carbon electrodes for lithium-ion batteries, J. Power Sources 183 (2008) 730–740, https://doi.org/10.1016/j.jpowsour.2008.05.065.
[22] J.H. Pikul, P.V. Braun, W.P. King, Performance modeling and design of ultra-high power microbatteries, J. Electrochem. Soc. 164 (2017) 3122–3131, https://doi.org/10.1149/2.0151711jes.
[23] H. Ning, J.H. Pikul, R. Zhang, X. Li, S. Xu, J. Wang, et al., Holographic patterning of high-performance on-chip 3D lithium-ion microbatteries, Proc. Natl. Acad. Sci. Unit. States Am. 112 (2015) 6573–6578, https://doi.org/10.1073/pnas.1423889112.
[24] H.D. Asfaw, M. Roberts, R. Younesi, K. Edström, Emulsion-templated bicontinuous carbon network electrodes for use in 3D microstructured batteries, J. Mater. Chem. A. 1 (2013) 13750–13758, https://doi.org/10.1039/c3ta12680c.
[25] H.D. Asfaw, M.R. Roberts, C.-W. Tai, R. Younesi, M. Valvo, L. Nyholm, et al., Nanosized LiFePO4-decorated emulsion-templated carbon foam for 3D micro batteries: a study of structure and electrochemical performance, Nanoscale 6 (2014) 8804–8813, https://doi.org/10.1039/C4NR01682C.
[26] R.A. Huggins, Advanced Batteries, 2009, https://doi.org/10.1017/CBO9781107415324.004. New York.
[27] Y. Wu, Lithium-ion Batteries Fundamentals and Applications, 2015. London.
[28] P.R. Shearing, L.E. Howard, P.S. Jørgensen, N.P. Brandon, S.J. Harris, Characterization of the 3-dimensional microstructure of a graphite negative electrode from a Li-ion battery, Electrochem. Commun. 12 (2010) 374–377, https://doi.org/10.1016/j.elecom.2009.12.038.
[29] M.D. Sarzynski, S. Schaefer, O.O. Ochoa, Microstructure-based models for multi-functional material systems, Mech. Adv. Mater. Struct. 6494 (2015) 421–430, https://doi.org/10.1080/15376494.2010.528166.
[30] S. Ackermann, J.R. Scheffe, J. Duss, A. Steinfeld, Morphological characterization and effective thermal conductivity of dual-scale reticulated porous structures, Materials (Basel) 7 (2014) 7173–7195, https://doi.org/10.3390/ma7117173.
[31] J. Liu, N.P. Wickramaratne, S.Z. Qiao, M. Jaroniec, Molecular-based design and emerging applications of nanoporous carbon spheres, Nat. Mater. 14 (2015) 763–774, https://doi.org/10.1038/nmat4317.
[32] D. Robert, T. Douillard, A. Boulineau, G. Brunetti, P. Nowakowski, D. Venet, et al., Multiscale phase mapping of LiFePO4-based electrodes by transmission electron microscopy and electron forward scattering diffraction, ACS Nano 7 (2013) 10887–10894, https://doi.org/10.1021/nn4043964.
[33] J.F. Rohan, M. Hasan, S. Patil, D.P. Casey, T. Clancy, Energy Storage : Battery Materials and Architectures at the Nanoscale, 2014.
[34] M.O. Steinhauser, S. Hiermaier, A review of computational methods in materials science: examples from shock-wave and polymer physics, Int. J. Mol. Sci. 10 (2009) 5135–5216, https://doi.org/10.3390/ijms10125135.
[35] S. Curtarolo, G.L.W. Hart, M.B. Nardelli, N. Mingo, S. Sanvito, O. Levy, The high-throughput highway to computational materials design, Nat. Mater. 12 (2013) 191–201, https://doi.org/10.1038/nmat3568.
[36] M.M. Kalantarian, S. Asgari, P. Mustarelli, Theoretical investigation of Li2MnSiO4 as a cathode material for Li-ion batteries: a DFT study†, J. Mater. Chem. A. 1 (2013) 2847–2855, https://doi.org/10.1039/c2ta01363k.
[37] Y. Gao, Z. Wang, L. Chen, Workfunction, a new viewpoint to understand the electrolyte/electrode interface reaction†, J. Mater. Chem. A. 3 (2015) 23420–23425, https://doi.org/10.1039/C5TA07030A.
[38] D. Brandell, P. Priimägi, H. Kasemägi, A. Aabloo, Branched polyethylene/poly (ethylene oxide) as a host matrix for Li-ion battery electrolytes: a molecular dynamics study, Electrochim. Acta 57 (2011) 228–236, https://doi.org/10.1016/j.electacta.2011.03.022.
[39] D. Brandell, A. Liivat, H. Kasemagi, A. Aabloo, J.O. Thomas, Molecular dynamics simulation of the LiPF6-PEO6 structure, J. Mater. Chem. (2005) 1422–1428, https://doi.org/10.1039/b417232a.
[40] C.-W. Wang, A.M. Sastry, Mesoscale modeling of a Li-Ion polymer cell, J. Electrochem. Soc. 154 (2007) A1035, https://doi.org/10.1149/1.2778285.
[41] M. Tang, P. Albertus, J. Newman, E. Energy, T. Division, L. Berkeley, Two-dimensional modeling of lithium deposition during cell charging, Electrochem. Soc. (2009) 390–399, https://doi.org/10.1149/1.3095513.
[42] V. Zadin, D. Brandell, Modelling polymer electrolytes for 3D-microbatteries using finite element analysis, Electrochim. Acta 57 (2011) 237–243, https://doi.org/10.1016/j.electacta.2011.03.026.
[43] K.H. Kwon, C.B. Shin, T.H. Kang, C.S. Kim, A two-dimensional modeling of a lithium-polymer battery, J. Power Sources 163 (2006) 151–157, https://doi.org/10.1016/j.jpowsour.2006.03.012.
[44] R.W. Hart, H.S. White, B. Dunn, D.R. Rolison, 3-D microbatteries, Electrochem. Commun. 5 (2003) 120–123, https://doi.org/10.1016/S1388-2481(02)00556-8.
[45] V. Zadin, H. Kasemägi, A. Aabloo, D. Brandell, Modelling electrode material utilization in the trench model 3D-microbattery by finite element analysis, J. Power Sources 195 (2010) 6218–6224, https://doi.org/10.1016/j.jpowsour.2010.02.056.
[46] P. Priimägi, D. Brandell, S. Srivastav, A. Aabloo, H. Kasemägi, V. Zadin, Optimizing the design of 3D-pillar microbatteries using finite element modelling, Electrochim. Acta 209 (2016) 138–148, https://doi.org/10.1016/j.electacta.2016.05.047.
[47] V. Zadin, D. Brandell, H. Kasemägi, A. Aabloo, J.O. Thomas, Finite element modelling of ion transport in the electrolyte of a 3D-microbattery, Solid State Ionics 192 (2011) 279–283, https://doi.org/10.1016/j.ssi.2010.02.007.
[48] P. Priimägi, H. Kasemägi, A. Aabloo, D. Brandell, V. Zadin, Thermal simulations of polymer electrolyte 3D Li-Microbatteries, Electrochim. Acta 244 (2017) 129–138, https://doi.org/10.1016/j.electacta.2017.05.055.
[49] D. Miranda, C.M. Costa, a. M. Almeida, S. Lanceros-Mendez, Computer simulations of the influence of geometry in the performance of conventional and unconventional lithium-ion batteries, Appl. Energy 165 (2016) 318–328, https://doi.org/10.1016/j.apenergy.2015.12.068.
[50] D. Miranda, C.M. Costa, A.M. Almeida, S. Lanceros-méndez, Computer simulation evaluation of the geometrical parameters affecting the performance of two dimensional interdigitated batteries, JEAC 780 (2016) 1–11, https://doi.org/10.1016/j.jelechem.2016.08.031.
[51] M. Doyle, T.F. Fuller, J. Newman, Modeling of galvanostatic charge and discharge of the lithium/polymer/insertion cell, Electrochem. Soc. 140 (1993) 1526–1533.
[52] R. Darling, J. Newman, Modeling a porous intercalation electrode with two characteristic particle sizes, J. Electrochem. Soc. 144 (1997) 4201–4208, https://doi.org/10.1149/1.1838166.
[53] T.R. Ferguson, M.Z. Bazant, Nonequilibrium thermodynamics of porous electrodes, J. Electrochem. Soc. 159 (2012) A1967–A1985, https://doi.org/10.1149/2.048212jes.
[54] K.A. Smith, C.D. Rahn, C.-Y. Wang, Control oriented 1D electrochemical model of lithium ion battery, Energy Convers. Manag. 48 (2007) 2565–2578, https://doi.org/10.1016/j.enconman.2007.03.015.
[55] W.A. van Schalkwijk, B. Scrosati, Advances in Lithium-ion Batteries, Springer US, Boston, MA, 2002, https://doi.org/10.1007/b113788.
[56] V. Srinivasan, J. Newman, Discharge model for the lithium iron-phosphate electrode, J. Electrochem. Soc. 151 (2004) 1517–1529, https://doi.org/10.1149/1.1785012.
[57] V. Srinivasan, J. Newman, Design and optimization of a natural graphite/iron phosphate, Electrochem. Soc. (2004) 1530–1538, https://doi.org/10.1149/1.1785013.
[58] M. Doyle, J. Newman, Comparison of modeling predictions with experimental data from plastic lithium ion cells, Electrochem. Soc. 143 (1996) 1890–1903.
[59] G. Dahlquist, Å. Björck, Numerical Methods in Scientific Computing, Volume I, 2007, https://doi.org/10.1039/c0cp90117b.
[60] R. Malik, A. Abdellahi, G. Ceder, A critical review of the Li insertion mechanisms in LiFePO4 electrodes, J. Electrochem. Soc. 160 (2013) A3179–A3197, https://doi.org/10.1149/2.029305jes.
[61] B. Ellis, L.K. Perry, D.H. Ryan, L.F. Nazar, Small polaron hopping in LixFePO4 solid solutions: coupled lithium-ion and electron mobility, J. Am. Chem. Soc. 128 (2006) 11416–11422, https://doi.org/10.1021/ja0614114.
[62] A. Samba, N. Omar, H. Gualous, O. Capron, P. Van den Bossche, J. Van Mierlo, Impact of tab location on large format lithium-ion pouch cell based on fully coupled tree-dimensional electrochemical-thermal modeling, Electrochim. Acta 147 (2014) 319–329, https://doi.org/10.1016/j.electacta.2014.08.115.
[63] S.L. Bewlay, K. Konstantinov, G.X. Wang, S.X. Dou, H.K. Liu, Conductivity improvements to spray-produced LiFePO4 by addition of a carbon source, Mater. Lett. 58 (2004) 1788–1791, https://doi.org/10.1016/j.matlet.2003.11.008.
[64] J. Molenda, A. Kulka, A. Milewska, W. Zając, K. Świerczek, Structural, transport and electrochemical properties of LiFePO4 substituted in lithium and iron sublattices (Al, Zr, W, Mn, Co and Ni), Materials (Basel) 6 (2013) 1656–1687, https://doi.org/10.3390/ma6051656.
[65] Y.-C. Chang, C.-T. Peng, I.-M. Hung, Effects of particle size and carbon coating on electrochemical properties of LiFePO4/C prepared by hydrothermal method, J. Mater. Sci. 49 (2014) 6907–6916, https://doi.org/10.1007/s10853-014-8395-9.
[66] J. Liu, M. Kunz, K. Chen, N. Tamura, T. Richardson, Visualization of charge distribution in a lithium-ion battery electrode, Meet. Abstr. 2 (2010) 208. http://ma.ecsdl.org/content/MA2010-02/4/208.abstract.

[67] F.C. Strobridge, B. Orvananos, M. Croft, H.-C. Yu, R. Robert, H. Liu, et al., Mapping the inhomogeneous electrochemical reaction through porous LiFePO 4 -electrodes in a standard coin cell battery, Chem. Mater. 27 (2015) 2374–2386, https://doi.org/10.1021/cm504317a.
[68] M.R. Roberts, A. Madsen, C. Nicklin, J. Rawle, M.G. Palmer, J.R. Owen, et al., Direct observation of active material concentration gradients and crystallinity breakdown in LiFePO 4 electrodes during charge/discharge cycling of lithium batteries, Phys. Chem. c. (2014) 6548–6557, https://doi.org/10.1021/jp411152s.
[69] M. Winter, R.J. Brodd, What are batteries, fuel cells, and supercapacitors? Chem. Rev. 104 (2004) 4245–4269, https://doi.org/10.1021/cr020730k.
[70] M. Ebner, V. Wood, Tool for tortuosity estimation in lithium ion battery porous electrodes, Electrochem. Soc. 162 (2015) 3064–3070, https://doi.org/10.1149/2.0111502jes.
[71] B. Orvananos, H. Yu, R. Malik, A. Abdellahi, C.P. Grey, G. Ceder, et al., Effect of a size-dependent equilibrium potential on nano-LiFePO4 particle interactions, J. Electrochem. Soc. 162 (2015) 1718–1724, https://doi.org/10.1149/2.0161509jes.
[72] Y. Li, S. Meyer, J. Lim, S.C. Lee, W.E. Gent, S. Marchesini, et al., Effects of particle size , electronic connectivity , and incoherent nanoscale domains on the sequence of lithiation in LiFePO4 porous electrodes, Adv. Mater. (2015) 6591–6597, https://doi.org/10.1002/adma.201502276.
[73] R. Shahid, S. Murugavel, Particle size dependent confinement and lattice strain effects in LiFePO4, Phys. Chem. Chem. Phys. (2013) 18809–18814, https://doi.org/10.1039/c3cp52953c.
[74] T.V.S.L. Satyavani, B.R. Kiran, V.R. Kumar, A.S. Kumar, S.V. Naidu, Effect of particle size on dc conductivity , activation energy and diffusion coefficient of lithium iron phosphate in Li-ion cells, Eng. Sci. Technol. an Int. J. 19 (2016) 40–44, https://doi.org/10.1016/j.jestch.2015.05.011.
[75] R. Malik, D. Burch, M. Bazant, G. Ceder, Particle size dependence of the ionic diffusivity, Nano Lett. 10 (2010) 4123–4127, https://doi.org/10.1021/nl1023595.